EurJIC European Journal of Inorganic Chemistry

ChemPubSoc Europe

FULL PAPER

DOI:10.1002/ejic.201300769

The Close Relationships between the Crystal Structures of MO and MSO_4 (M = Group 10, 11, or 12 Metal), and the Predicted Structures of AuO and $PtSO_4$

Mariana Derzsi,*[a] Andreas Hermann,[b,c] Roald Hoffmann,[b] and Wojciech Grochala[a,d]

Dedicated to the memory of Detlef Schröder

Keywords: Metal oxides / Metal sulfates / Transition metals / Structure elucidation / Jahn–Teller distortion

The structural relations of (and between) late transition metal monoxides, MO, and monosulfates, MSO_4, are analyzed. We show that all of these late transition metal oxides, as well as 4d and 5d metal sulfates, crystallize in distorted rock salt lattices and argue that the distortions are driven by collective first- and/or second order Jahn–Teller effects. The collective Jahn–Teller deformations lead either to tetragonal contraction or (seldom) elongation of the rock salt lattice. On the basis of the rock salt representation of the oxides and sulfates, we show that PdO, CuO, and AgO are metrically related and that the 4d and 5d metal sulfates are close to isostructural with their oxides. These observations guide us towards as yet unknown AuO and $PtSO_4$, for which we predict crystal structures from electronic structure calculations.

Introduction

Solids containing late transition metal (LTM; i.e., group 10, 11, or 12) cations are known to exhibit a broad range of fascinating physicochemical properties. These encompass rich polymorphism, collective first- or second-order Jahn–Teller (JT) effects[1] in their crystal lattices, strong magnetic superexchange between metal centers that often leads to antiferromagnetism (especially for d^9 and high-spin d^8 systems), metallic conductivity and even superconductivity (for mixed-valence compositions), and thermochromism (mostly for d^{10} systems).

The properties in question arise from strong electronic correlations of the d electrons at metal centers (for d^8 and d^9 configurations) and from flexibility of the coordination sphere of the metal cation—be it due to a first-order (for d^9 and low-spin d^8 electronic configurations) or second-order JT effect (for a d^{10} configuration). The most intensely studied systems in this family are the oxides (MO), sulfides (MS), and sulfates (MSO_4) of divalent metals. These prototypical LTM compounds provide a rich source of research problems for both experimental and theoretical investigation, and they continue to fascinate solid-state physicists and chemists alike.[2]

The purpose of this study is to demonstrate that the polymorphism of the LTM metal monoxides and monosulfates is a direct manifestation of the aforementioned JT effect and/or relativistic effects for the heaviest elements in this set.[3] A common structural type among the early transition metal monoxides (groups 4–6) as well as among most of the 3d (groups 4–10) monoxides is the rock salt (NaCl-type) structure. However, among the LTM monoxides, only CdO is known to take up the ideal rock salt structure under ambient (*p*, *T*) conditions, whereas the remaining LTM monoxides MO (M = Pd, Pt, Cu, Ag, Zn, Hg) all crystallize in different crystallographic systems (Table 1; for cell parameters see Table S2, Supporting Information). The known transition metal monosulfates are limited to 3d (groups 7–12) and LTM 4d (M = Pd, Ag, Cd) and 5d (M = Pt, Hg) monosulfates, and none of them crystallize in a rock salt type structure. Similarly, as in the case of 3d monoxides, the 3d metal monosulfates adopt the same crystal structure types, orthorhombic *Cmcm* ($CrVO_4$-type) and/or *Pnma* ($CuSO_4$-type) cell ($Z = 4$), whereas again the LTM monosulfates all crystallize in distinct space groups (Table 1; for cell parameters see Table S2, Supporting Information).

In the following, we demonstrate that although different in details, the LTM monoxides and 4d/5d monosulfates can

[a] Laboratory of Technology of Novel Functional Materials, Center for New Technologies, University of Warsaw, ul. Żwirki i Wigury 93, 02-089 Warsaw, Poland
E-mail: mariana@cent.uw.edu.pl
Homepage: ltnfm.icm.edu.pl
[b] Department of Chemistry and Chemical Biology, Cornell University, Ithaca NY, 14853 USA
[c] School of Physics and Astronomy, University of Edinburgh, Edinburgh, EH9 3JZ, United Kingdom
[d] Faculty of Chemistry, University of Warsaw, Pasteur 1, 02-093 Warsaw, Poland

Supporting information for this article is available on the WWW under http://dx.doi.org/10.1002/ejic.201300769.

Table 1. All known polymorphs of late-transition metal monoxides (MO) at room temperature (the only exception is hexagonal ZnO at 19 K) and monosulfates (MSO_4). T_N is the Néel temperature, whereas HP, HT, and LT stand for high pressure, high temperature, and low temperature, respectively. meta = metastable. The listed volumes, V, are calculated per formula unit $Z = 1$.

Monoxides (MO)				Monosulfates (MSO_4)			
MO	Space group	V [Å^3]	Z	MSO_4	Space group	V [Å^3]	Z
NiO	$R\bar{3}m^{<T_N}$	18.21[4]		$NiSO_4$	$Cmcm$	64.06[5]	4
	$Fm\bar{3}m^{>T_N}$	18.13[6]	4				
CuO	$C2/c$	20.76[7]	4	$CuSO_4$	$Pnma$	68.17[8]	4
ZnO	$P6_3/mc$	23.75[19K][9]	2	$ZnSO_4$	$Pnma^{LT}$	69.28[8]	4
	$Fm\bar{3}m^{HP}$	19.60[10]	4		$F\text{-}43m^{HT}$	92.38[11]	4
PdO	$P4_2/mmc$	24.22[12]	2	$PdSO_4$	$?^{LT}$	75.52[13]	16
	$I4/mmm^{HP[a]}$	23.94[14]	2		$C2/c^{HT}$	79.95[13]	4
AgO	$P2_1/c$	26.67[15]	4	$AgSO_4$	$C2/c$	75.86[16]	16
	$I4_1/a$	26.62[17]	16				
CdO	$Fm\bar{3}m$	25.94[18]	4	$CdSO_4$	$Pn2_1m$	72.70[19]	2
	$Pm\bar{3}m^{HP}$	≈17.8[b][20]	1		$Cmcm^{HT1}$	77.75[21]	4
					$P\bar{3}m1^{HT2}$	83.07[22]	2
PtO	$P4_2/mmc$	24.68[12]	2	$PtSO_4$[d]			
HgO	$Pnma$	32.15[23]	4	$HgSO_4$	$Pn2_1m$	75.91[24]	2
	$P\bar{1}$-meta[c]	32.28[25]	8				
	$P3_121$-meta	32.26[26]	3				
	$I4/mmm^{HP1}$	26.41[27]	2				
	$Fm\bar{3}m^{HP2}$	≈25[b][28]	4				
AuO[d]				$AuSO_4$	$Pbca$	88.25[29]	8

[a] Likely nonstoichiometric. [b] Derived from the published equation of state. [c] Structurally very close to *Pnma*. [d] Not known at the time of writing.

all be viewed as crystallizing in distorted rock salt lattices, and throughout the text they are discussed in their rock salt type representations. The transformation into a rock salt type representation for each of these compounds is achieved by multiplication of the corresponding 3×3 matrix **A** (which represents lattice vectors in a Cartesian system) by an appropriate 3×3 transformation matrix **T**. The resulting matrix **A′** = **AT** represents lattice vectors of the rock salt type cell. As an example, consider the tetragonal AgO structure ($I4_1/a$) with $a = b = 6.833$ Å, $c = 9.122$ Å, $\alpha = \beta = \gamma = 90°$. Thus, the Cartesian matrix **A** = [**a**,**b**,**c**], in which **a** = (6.833, 0.0, 0.0), **b** = (0.0, 6.833, 0.0), and **c** = (0.0, 0.0, 9.122). The transformation matrix **T** = [(1,1,0) (1,–1,0) (0,0,–1)] transforms the initial Cartesian matrix **A** into a new one **A′** = [(9.664, 0.0, 0.0), (0.0, 9.664, 0.0), (0.0, 0.0, 9.122)] (which corresponds to $a' = b' = 9.664$ Å, $c' = 9.122$ Å, $\alpha' = \beta' = \gamma' = 90°$).

The structural distortions of MO and MSO_4 are rationalized on the basis of collective JT effects. Similarities and differences between the distortions in the monoxides and monosulfates are highlighted, and structural relations between them are revealed. Guided by the striking similarities we find among these materials and by using quantum mechanical DFT calculations, we end our study by proposing crystal structures for the only unknown LTM monoxide and monosulfate, AuO and $PtSO_4$, respectively.

Results and Discussion

Monoxides

The crystal structures of all LTM oxides in the rock salt representations are compared in Figure 1 and the transformed crystal lattice parameters (a', b', c', α', β', γ') are

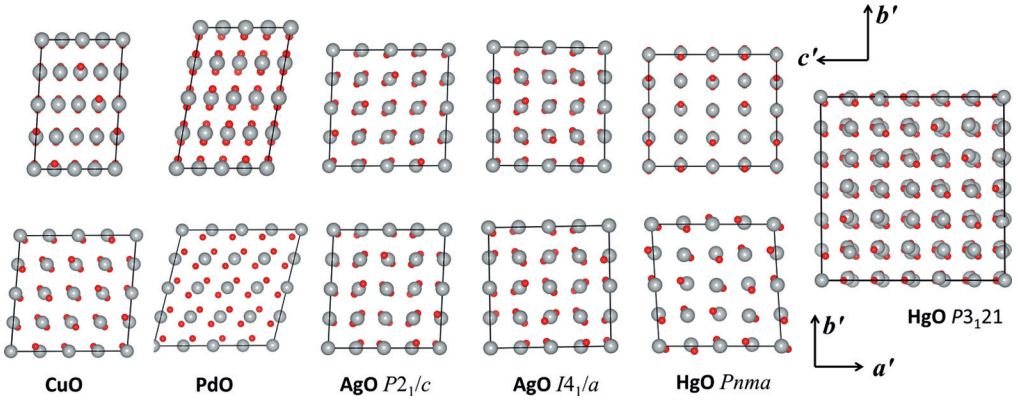

Figure 1. Late transition metal oxides MO transformed into rock salt representations. (Top) View along a'(= b'), (bottom) view along c'. In the case of HgO $P3_121$, $a' = b' = c'$ and all projections are identical. For the matrix transformations see Table S2, Supporting Information.

Table 2. Rock salt type $2\times2\times2$ supercell representations of all known late transition metal oxides MO and 4d/5d monosulfates both listed with respect to increasing c'/a' ratio. For the transformation matrices see Table S2, Supporting Information.

Structure	c'/a'	a' [Å]	b' [Å]	c' [Å]	α' [°]	β' [°]	γ' [°]
PdO	0.62	10.927	10.927	6.815	97.68	90	102.85
PtO	0.62	10.997	10.997	6.856	97.65	90	102.86
CuO	0.63	10.104	10.104	6.318	93.99	90	84.91
AgO $P2_1/c$	0.95	9.669	9.669	9.153	92.62	90	92.01
AgO $I4_1/a$	0.94	9.664	9.664	9.122	90	90	90
HgO^{HP1}	0.98	9.532	9.532	9.302	90	90	90
NiO^{HT}	1	8.340[a]	8.340[a]	8.340[a]	90	90	90
ZnO^{HP}	1	8.56[a]	8.56[a]	8.56[a]	90	90	90
CdO	1	9.398[a]	9.398[a]	9.398[a]	90	90	90
HgO^{HP2}	1	9.28[a]	9.28[a]	9.28[a]	90	90	90
HgO $P3_121$	1	10.086[b]	10.086[b]	10.086[b]	89.65	90	90.35
HgO *Pnma*	1.14	9.662	9.662	11.042	90	90	93.61
HgO $P\bar{1}$	1.15	9.629	9.629	11.080	90.63	90	86.98
$PdSO_4^{HT}$	0.79	14.808	14.808	11.672	89.66	89.66	88.78
$PdSO_4^{LT}$	0.89	13.979	13.979	12.382	90	90	90.04
$AgSO_4$	0.94	13.828	13.669	12.848	90	90,86	90
$HgSO_4$	0.97	13.585	13.585	13.162	90	90	90.42
$CdSO_4$	0.99	13.318	13.318	13.116	90	90	90.3

[a] A smaller $1\times1\times1$ rock salt type cell can be generated. [b] a' is listed as 2/3 of the unit cell vector of the $3\times3\times3$ cell.

listed in Table 2 (for transformation matrices, see Table S2, Supporting Information). The respective atomic displacements (in fractional coordinates) relative to the atomic positions in the rock salt structure are listed in Table 3 (and Table S3, Supporting Information). Doubling of the rock salt cell in all three crystallographic directions ($2\times2\times2$) is required to accommodate these distortions of the atomic positions. The only exception is the HgO $P3_121$ form; here, the atomic displacements occur in a $3\times3\times3$ supercell of the rock salt unit cell.

The transformed lattice parameters (Table 2) point to quasitetragonal deformations in almost all of these structures, as $a' = b' \neq c'$, whereas the unit cell angles remain close to 90°. It is also apparent from the c'/a' ratios that tetragonal distortion has a different character in PdO, PtO, CuO, AgO, and tetragonal HgO-HP (*I*4/*mmm*) on the one hand, and in the HgO *Pnma* and $P\bar{1}$ phases on the other hand. The former experience tetragonal contraction ($a' = b' > c'$), whereas the latter experience tetragonal elongations ($a' = b' < c'$). The tetragonal contraction is most pronounced for PdO, PtO, and CuO, with their very low c'/a' ratios of 0.62, 0.62 and 0.63, respectively. In PdO and PtO, the γ' angle is additionally distorted from 90° by as much as 13° (in the remaining cases the deviation is smaller than 5°). AgO, in contrast, experiences the smallest tetragonal contraction, and the c'/a' ratio is 0.95 and 0.94 for the monoclinic and tetragonal polymorphs, respectively. HgO provides the only tetragonally elongated rock salt types with c'/a' ratios of 1.14 and 1.15 for the *Pnma* and $P\bar{1}$ forms, respectively. The cinnabar polymorph of HgO ($P3_121$) is an exception, as it does not experience any metrical unit cell distortion except for a tiny angular one (<0.5°).

Structural departure of the LTM monoxides from the rock salt structure type is a direct manifestation of the collective JT effects. It is well understood that in an octahedral environment, the d^8 (low-spin Pd^{2+} and low-spin Ag^{3+}) and d^9 (Cu^{2+}) ions experience local first-order JT effect-driven elongation along the octahedral z axis; the doubly occupied $d(z^2)$ orbital is stabilized over the empty (for d^8) or half-occupied (for d^9) $d(x^2–y^2)$ orbital. Therefore, the axial ligands involved in metal–ligand antibonding with the $d(z^2)$ orbital move away. As a result, these ions always show an effectively square-planar or an elongated octahedral first coordination sphere, with four short covalent equatorial M–O bonds and two long or no axial M–O contacts. If we now examine the orientation of the $[MO_6]$ octahedra in the tetragonally contracted rock salt representations of PdO, PtO, CuO, and AgO, we find that the preferred orientation of the octahedral z axis [i.e., the collective alignment of the $d(z^2)$ orbitals] is along the a' and b' axes, that is, the directions of two long lattice vectors. The four short M–O bonds, defining the orientation of the $d(x^2–y^2)$ orbitals, thus reside in the $b'c'$ and $a'c'$ planes (Figure 2, top left). As a result, the c' direction contains only short M–O bonds, whereas within the $a'b'$ plane short and long M···O contacts alternate. This is consistent with a tetragonal contraction of the rock salt lattice along c'.

The cation–anion connectivity in AgO is additionally complicated by the simultaneous presence of the d^{10} (Ag^{1+}) and d^8 (Ag^{3+}) cations (it is a mixed-valence compound; its proper formula is $Ag^{I}Ag^{III}O_2$). The d^{10} ions, in general, show linear or tetrahedral coordination. The linear geometry (compressed octahedron) can be viewed as an outcome of a strong "inverse"[30] second-order JT effect resulting from $d(z^2)$/s mixing. In both AgO polymorphs, the short octahedral z axis of the Ag^{1+} ions aligns along the same directions (alternatively along a' and b') as the elongated octahedral z axis of Ag^{3+} (Figure 2, top right). Thus, the inverse second-order JT effect compensates for the first-order one. As a result, the tetragonal distortion of the rock salt lattice is much smaller in both forms of AgO (c'/a' = 0.94–0.95) than in PdO and CuO (c'/a' = 0.62–0.63). The cancelation of the two effects is, however, not complete because the second-order JT effect for Ag^{1+} is smaller than

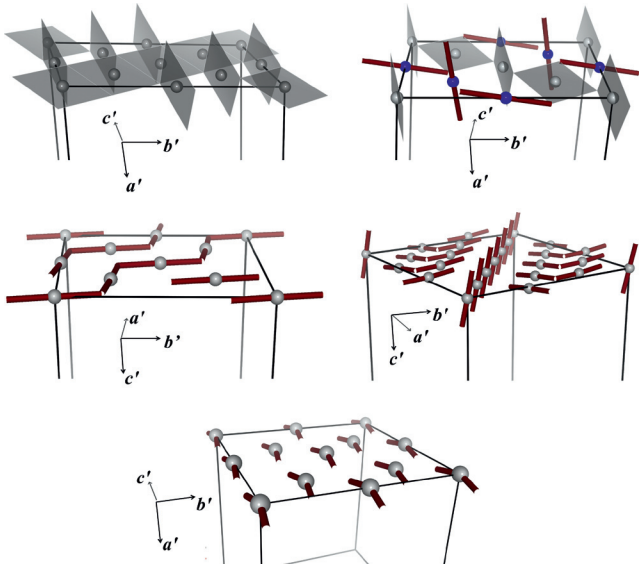

Figure 2. Illustration of the orientation of the d(x^2–y^2) (square-planar coordination spheres) and d_{z^2} orbitals (linear coordination sphere) in LTM monoxides and monosulfates: CuO, PdO, PtO, $PdSO_4$, $AgSO_4$ (top left); both forms of AgO (top right); HgO *Pnma* (middle left); HgO $P3_121$ (middle right); and $CdSO_4$ and $HgSO_4$ (bottom). The relative orientation of the coordination spheres in successive layers is the same. See text for details.

the first-order JT effect for Ag^{3+}. Notably, the d(z^2) (Ag^{1+}) and d(x^2–y^2) (Ag^{3+}) orbitals in AgO show the same ferrodistortive alignment along the (0,1,1) direction ($b'c'$ diagonal) as the d(x^2–y^2) (M^{2+}) orbitals in CuO, PdO, and PtO. Upon considering the second-shortest Ag^{1+}–O bonds in the first coordination sphere of Ag^{1+} in both AgO forms, the same structural connectivity within the $b'c'$ planes would result, as in the case of the former (d^8 and d^9) monoxides.

In the two ambient pressure forms of HgO (*Pnma* and $P\bar{1}$), the collective inverse second-order JT effect for the Hg^{2+} cations acts in the same directions as it does for Ag^{1+} in AgO (along a' and b'). Hence, tetragonal elongation along c' of its rock salt lattice is observed (c'/a' = 1.14–1.15), with the zigzag Hg–O chains running along the diagonal of the $a'b'$ plane (Figure 2, middle left). The d/s mixing in Hg^{2+} is, of course, considerably stronger than that in Ag^{1+} as a result of the relatively stabilized 6s orbital of Hg.[31] In the cinnabar structure of HgO, stabilization of the d(z^2) orbital over the d(x^2–y^2) orbital takes place alternatively along all three crystallographic directions (a', b', c'; Figure 2, middle right); therefore, the distortions of the rock salt cell are isotropic ($c'/b'/a'$ = 1). This is realized by spiral-like Hg–O chains running along the body diagonal of the rock salt type cell. In the HgO-HP1 form (*I*4/*mmm*), in contrast, the compressed [HgO_{2+4}] octahedra have their short axes aligned parallel to c', which leads to a slight compression of the rock salt type cell along this axis (c'/a' = 0.98).

Monosulfates

As mentioned earlier, all 3d TM monosulfates commonly adopt two closely related orthorhombic forms (*Cmcm* and *Pnma*) with simple hexagonal NiAs-type MS sublattice (see Figure S6, Supporting Information). The situation is different in the 4d and 5d LTM monosulfates. Although they crystallize in distinct crystallographic systems, all but one ($AuSO_4$) can be viewed as distorted rock salt type lattices containing 32 formula units, with metal and sulfur atoms occupying (approximately) the special positions in the rock salt lattice (Figure 3). For these $2\times2\times2$ supercells, $a' = b' > c'$ ($a' \approx b' > c'$ for $AgSO_4$), and unit cell angles deviate from 90° by less than 3° (Table 2). In all cases, $c'/a' < 1$, that is, the rock salt type cell is tetragonally contracted.

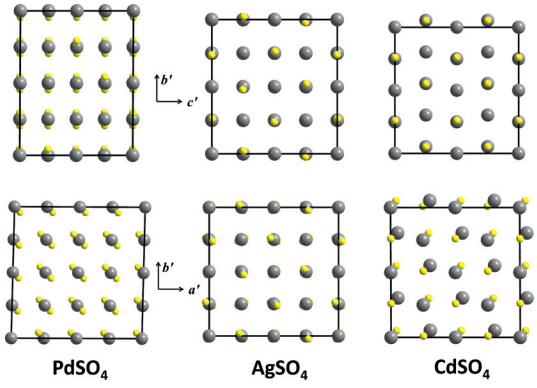

Figure 3. The 4d late transition metal sulfates $M^{II}SO_4$ in their $2\times2\times2$ rock salt type representations viewed along the a'(= b') axis (top) and the c' axis (bottom). In $AgSO_4$, $a' \approx b'$ and the views along both axes are comparable. $HgSO_4$ is isostructural with $CdSO_4$. Atoms: metal (large gray), S (small yellow). Oxygen atoms were omitted.

These deformations are reminiscent of those in the LTM monoxides, which also experience tetragonal distortions of the rock salt lattice (Table 2), and the atomic displacements follow very similar patterns to those observed for the LTM sulfates (Table 3). Most clear is the resemblance of $PdSO_4$ to PdO. Both feature a tetragonally contracted rock salt lattice with the light atoms displaced only within the tetragonal $a'b'$ plane, whereas the number (two) and directions of the nonequivalent displacements are the same in both. Comparing the PdO and PdS (sub)lattices, it is evident that the only quantitative difference between them is the larger γ' angle in the case of the oxide. $AgSO_4$ can, in this respect, also be compared to the two silver oxide structures. All of them are tetragonally contracted rock salt lattices with anions displaced along all three crystallographic directions. However, it is tetragonal AgO that shows closer relation to $AgSO_4$. The number and direction of the displacements is the same in both (Table 3).

Finally, comparing the structural deformations in $HgSO_4$ and the three known HgO forms, some resemblance is observed between the sulfate and orthorhombic HgO. Although the oxide experiences tetragonal elongation rather than tetragonal contraction (as observed in $HgSO_4$, Table 2), in both structures the atomic displacements take place only within the tetragonal $a'b'$ plane, and only every second metal atom is displaced within the plane (Table 3, we neglect the vanishing distortions of the remaining metal atoms in the oxide).

Table 3. Atomic displacements, Δ, (in fractional coordinates of the $1 \times 1 \times 1$ cell) from exact positions in the rock salt type representations of late transition metal monoxides MO and MS sublattice of late transition metal monosulfates MSO_4. The number of displacements is equal to the number of formula units in the original primitive cell of the respective oxide or sulfate.

Structure	Δx	Δy	Δz	Atom	Position
PdO	0.125	–0.125	0	O	all[a]
	–0.125	0.125	0		
$PdSO_4^{HP}$	0.086	–0.086	0	S	all[a]
	–0.086	0.086	0		
AgO $I4_1/a$	0.067	–0.093	0.074	O	(0, 0, 1/2)
	–0.067	0.093	–0.074		
	0.067	–0.093	–0.074	O	(1/2, 1/2, 1/2)
	–0.067	0.093	0.074		
	0.093	0.067	–0.074	O	(1/2, 0, 0)
	–0.093	–0.067	0.074		
	0.093	0.067	0.074	O	(0, 1/2, 0)
	–0.093	–0.067	–0.074		
$AgSO_4$	–0.054	0.026	0.006	S	(0, 1/2, 0)
	0.054	–0.026	–0.006		
	0.054	0.026	–0.006	S	(1/2, 1/2, 1/2)
	–0.054	–0.026	0.006		
	–0.034	–0.045	–0.007	S	(1/2, 0, 0)
	0.034	0.045	0.007		
	–0.034	0.045	–0.007	S	(0, 0, 1/2)
	0.034	–0.045	0.007		
HgO *Pnma*	0	0	0	Hg	(0, 0, 0; 1/2, 1/2, 0)
	–0.004	0.004	0		
	0.023	0.023	0	Hg	(1/2, 0, 1/2; 0, 1/2, 1/2)
	0.018	0.027	0		
	0.071	–0.079	0	O	(0, 1/2, 0; 1/2, 0, 0)
	–0.084	0.075	0		
	0.102	–0.048	0	O	(0, 0, 1/2; 1/2, 1/2, 1/2)
	–0.052	0.107	0		
$HgSO_4$	0.078	–0.08	0	Hg	(0, 1/2, 1/2; 1/2, 0, 1/2)
	0.001	–0.001	0	S	(0, 1/2, 0; 1/2, 0, 0)
	0.077	–0.077	0	S	(0, 0, 1/2; 1/2, 1/2, 1/2)

[a] Displacements are from all symmetry-equivalent exact positions.

The tetragonal contraction of the rock salt lattice observed in $PdSO_4$ and $AgSO_4$ is due to the same antiferrodistortive alignment of the specially expanded JT-active $d(z^2)$ orbitals within the $a'b'$ plane as that in CuO, PdO, and PtO (Figure 2, top left). Notably, $AgSO_4$ is a d^9 compound and it experiences the same alignment of the $d(z^2)$ orbitals as that in the d^9 monoxide CuO as well as in d^8 PdO and PtO [all of which experience strong stabilization of the $d(z^2)$ orbitals]. In $CdSO_4$ and $HgSO_4$, the tetragonal contraction emerges as a result of the alignment of, in this case, specially contracted $d(z^2)$ (inverse JT effect in d^{10} cations) along the c' vector (ferrodistortive alignment; Figure 2, bottom). This is in contrast to all three forms of HgO, in which the $d(z^2)$ orbitals orient alternatively either along the a' and b' axes (tetragonal elongation in *Pnma* and $P\bar{1}$; Figure 2, middle left) or along all three a', b', and c' axes (rhombohedral distortion in $P3_121$; Figure 2, middle left).

MO versus MSO_4

We demonstrated above that the crystal structures of LTM monoxides and monosulfates can be viewed as tetragonally distorted rock salt type lattices (the only exception is the HgO cinnabar structure with rhombohedrally distorted rock salt type lattice) and that tetragonal contraction in the d^8 and d^9 monoxides and monosulfates emerges out of the same antiferrodistortive alignment of the $d(z^2)$ orbitals that is found in all of them.

In the following, we demonstrate that the primitive cells for both families of compounds can be compared directly to reveal identical topologies of cationic and anionic sublattices (Figure 4). It turns out that one can obtain the structures of 4d/5d metal sulfates simply by substituting the oxygen atoms in the respective monoxides with SO_4 groups. Apart from clear changes in space group symmetry (local symmetry at the anionic site must decrease to tetrahedral, at best), cell parameters, and the presence of various small distortions, the topology and connectivity of the crystal network is not qualitatively affected by such a substitution. The four oxygen p orbitals of the SO_4^{2-} anion take the same role in bonding to the nearest four metal cations as that of the four hybridized sp^3 orbitals of the O^{2-} anions in the respective LTM monoxides. There is only one qualitative difference. The oxygen linker in the oxides is replaced by the $–SO_2$ fragment of the SO_4 group in the sulfates. Thus, the ···M–O–M–O··· network is replaced by a ···M–[O–S–O]–M–[O–S–O]··· one.

Let us begin a more detailed analysis with PdO versus $PdSO_4$. At first glance, these two compounds crystallize in distinct crystal structures (tetragonal and monoclinic, respectively), with distinct Z (2 and 4, respectively). How-

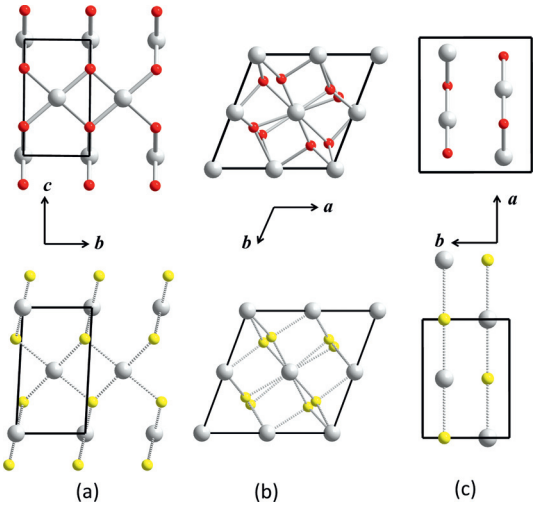

Figure 4. Primitive cells of LTM oxides (top) and sulfates (bottom, oxygen atoms omitted) of (a) Pd, (b) Ag in which AgO $I4_1/a$, and (c) Hg highlighting the structural relationship between the oxides and MS sublattices of the respective sulfates. In the bottom panel each metal cation is connected to the four closest S atoms that donate their oxygen atoms. One oxygen atom is located between each such M···S pair. Atoms: metal (large gray), S (small yellow), O (small red).

ever, if we focus on the content of the primitive cells, we see that within them the metal ions occupy identical positions and that the sulfate anions in $PdSO_4$ are only slightly displaced relative to the O^{2-} ions in PdO (Figure 4, a). The primitive cell vectors grow by $\Delta a = \Delta b = 1.68$ Å and $\Delta c = 2.599$ Å under such substitution, and the successive metal layers running parallel to the *c* axis drift slightly ($\Delta\gamma = -23°$, Table 4) to accommodate the new links.

Table 4. Comparison of the primitive cell parameters for structurally related sulfates and oxides. In the case of $HgSO_4$, parameters of the $2\times1\times1$ supercell are listed (see text for details).

	a [Å]	*b* [Å]	*c* [Å]	$\alpha = \beta$ [°]	γ [°]
PdO	3.020	3.020	5.310	90	90
$PdSO_4$	4.700	4.700	7.909	94.68	66.87
AgO $I4_1/a$	6.644	6.644	6.644	61.89	93.3
$AgSO_4$	9.380	9.380	9.508	62.48	93.5
HgO	6.613	5.521	3.522	90	90
$HgSO_4$	13.162[a]	4.785	4.821	90	90

[a] Value of $2\times a$ is shown.

Concerning $AgSO_4$, its crystal structure may be directly related to tetragonal AgO (Figure 4, b). Both feature $Z = 8$ (in primitive cells), $a = b < c$, the lattice angles are almost identical, and the increase in the lattice vectors, going from the oxide to the sulfate, is nearly isotropic (Table 4). These observations suggest that, in comparison to PdO, even smaller distortions of the AgO structure take place upon $O^{2-}\rightarrow SO_4^{2-}$ replacement. Although the two views in Figure 4 (b) emphasize the same crystal networks in both structures, there is an important chemical difference between the two. In AgO, two silver cations, Ag^{III} and Ag^{I}, are present, whereas the more acidic sulfate environment stabilizes silver in the intermediate oxidation state Ag^{II}. Comparison of the two primitive cells reveals that the $O^{2-}\rightarrow SO_4^{2-}$ replacement accompanied by the $Ag^{1+}/Ag^{3+}\rightarrow Ag^{2+}$ comproportionation does not require reorientation of the metal coordination spheres but mainly contraction of the $[Ag^{I}O_6]$ octahedra.

$HgSO_4$ is the remaining LTM sulfate that can be associated with its monoxide (Figure 4, c). As shown in the previous section, $HgSO_4$ most resembles the orthorhombic form of HgO. The structure of orthorhombic HgO consists of infinite zigzag –Hg–O– chains lying within the *ac* plane and running along the *a* direction, the longest lattice vector. In $HgSO_4$, the zigzag –Hg–O– chains are replaced by close-to-linear –Hg–O–S–O– ones. The $O^{2-}\rightarrow SO_4^{2-}$ replacement leads to a strong anisotropic expansion of the orthorhombic *Pnma* cell along the longest unit cell direction (lattice vector *a*) by a factor of approximately 2. The unit cell is, however, reduced along *a* by a factor of 2 owing to symmetry, as the space group changes from *Pnma* ($Z = 4$) for the oxide to $Pn2_1m$ ($Z = 2$) for the sulfate. Therefore, the magnitude of the *a* vector in the oxide must be compared to value of $2\times a$ in the sulfate (Table 4). The contraction of the *b* vector by –0.74 Å as well as a relatively small increase in *c* by 1.3 Å reflect the fact that additional short contacts are formed between the infinite chains in the sulfate (not shown).

Given that the sulfate anion is much larger than the oxide anion, it may seem puzzling that sulfates may be structurally related to their corresponding oxides (as this clearly violates Pauling's rules[32]). Similarities between MO and the corresponding MSO_4 systems also seem to contradict Bastide's structural diagram.[33] We think that the strong covalent character of LTM–oxygen bonds,[34] which is most pronounced for LTMs, the dominant role of JT distortions, and the (rotational) flexibility of the sulfate anion are all jointly responsible for the remarkable crystallochemical similarity between the MO and MSO_4 systems. Moreover, Vegas and Jansen's observations[35] concerning the isotypical character of metal sulfates and the corresponding sulfides rarely apply to LTM systems, and these cases should be treated as exceptions rather than confirmations of the rule.

From Known to Unknown LTM Compounds

We showed above that the crystal structures of 4d/5d LTM monoxides and monosulfates are directly related, and we used these findings to predict the crystal structures of AuO and $PtSO_4$ through quantum mechanical calculations. AuO and $PtSO_4$ are the only LTM monoxide and monosulfate, respectively, not known. To our best knowledge, they have not yet been prepared and no theoretical studies have been performed to predict their possible crystal structures. According to the structural relationships observed between the remaining 4d/5d monoxides and their monosulfates, AuO should adopt a crystal structure of the $AuSO_4$ type. However, recalling that 4d compounds and their 5d variants often adopt the same crystal structures (e.g., PdO versus

PtO and $CdSO_4$ versus $HgSO_4$), one expects that AuO should be a mixed-valence compound much like AgO.

In the case of $PtSO_4$, both approaches lead to only one candidate. Given that PtO crystallizes in the same structure as PdO and that we showed that $PdSO_4$ is related to PdO, we expect that $PtSO_4$ will crystallize in the very same structure as $PdSO_4$. This suggestion is supported by our theoretical calculations, which show that $PtSO_4$ is dynamically stable (Figure S8, Supporting Information) in the $PdSO_4$-type structure with unit cell parameters a = 7.033 Å, b = 6.750 Å, c = 7.609 Å, and β = 103.8° (theoretical crystal structure data in Table S8, Supporting Information). The only other reasonable candidate—the $AgSO_4$-type structure (the only remaining LTM sulfate with M^{2+} in square-planar coordination)—was found to be 55 meV per formula unit higher in energy. We expect that $PtSO_4$ will be stable in the $PdSO_4$-type structure under ambient (p, T) conditions. Support for this contention comes from the fact that Pd and Pt are among the most closely related elements in the periodic table often forming isostructural compounds (such as oxides and halides).

Our calculations performed for AuO show that disproportionated AuO in both AgO polytypes is energetically favored over the comproportionated CuO structure by 172 meV (AgO $P2_1/c$) and 127 meV (AgO $I4_1/a$) per formula unit (FU). Out of the two AgO-type forms, only the AgO $P2_1/c$ type (lattice parameters in Table 5 and structural data in Table S9, Supporting Information) was found to be dynamically stable (Figure S8, Supporting Information).

The $AuSO_4$-type starting model led us to four dynamically stable polymorphs (energetically they differ by at most ΔE = 45 meV FU^{-1}). Lattice parameters for the lowest-energy layered $P2_1/c$ polymorph are illustrated in Table 5 (for dispersion curves and crystal structure data see Figure S8 and Table S9 in Supporting Information, respectively). All four forms are layered structures with slightly puckered layers and Au^{2+}–Au^{2+} dimers that are reminiscent of $AuSO_4$; they differ only in stacking of the successive layers. One such layer of the lowest-energy 2D polymorph is compared with the respective layer of $AuSO_4$ in Figure 5 (left). The Au–Au bond length is as short as 2.57 Å for the layered AuO form, compared to the experimentally observed value of 2.490 Å in $AuSO_4$. Energetically, the layered $P2_1/c$ polymorph is, however, disfavored with respect to the two 3D AgO $P2_1/c$-type structures by 63 meV FU^{-1}. This is a further piece of evidence that suggest the preference of AuO for disproportionation.

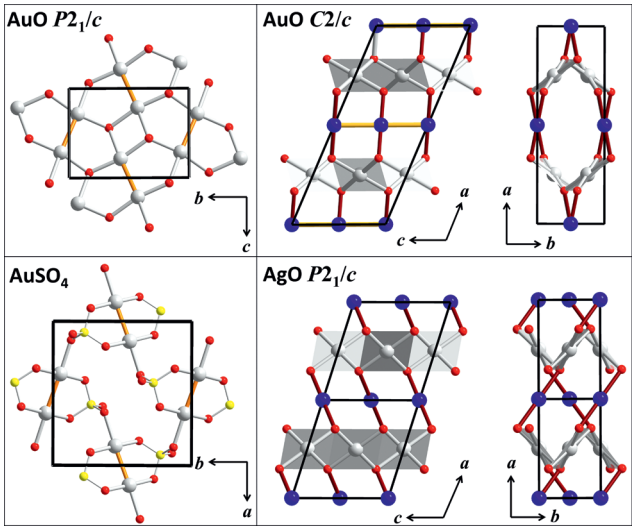

Figure 5. Two of the theoretically predicted dynamically stable polymorphs of AuO (top) compared to experimentally observed $AuSO_4$ and AgO structures (bottom). Color legend: M^{2+} and M^{3+} (light grey), M^{1+} (dark blue), O (red).

Interestingly, a structure search performed with the use of evolutionary algorithms,[36] designed to find global minima, revealed a new structure that was not accessible by following imaginary or low-frequency phonon modes of known structure types: a distinct, yet still disproportionated $C2/c$ structure (ground state at p = 1 atm, 1 atm = 101.3 kPa). This unique polymorph consists of a 3D $Au^{1+}Au^{3+}O_2$ network in which Au^{1+} and Au^{3+} are found in their common coordination environments, linear and square-planar, respectively. Each type of cation is found in a separate bc layer, a feature reminiscent of monoclinic AgO (compare the top and bottom views in Figure 5, right). The Au^{1+} ions in the $C2/c$ structure are additionally mutually linked by aurophilic interactions [d(Au–Au) = 2.77 Å] into infinite linear chains running along the c axis.[37] The aurophilic interactions are an important stabilizing factor, as the energy of the $C2/c$ structure is 42 meV FU^{-1} lower than that of the monoclinic AgO-type for which aurophilic interactions are absent.

The $C2/c$ structure of AuO can be thought of as being derived from AgO $P2_1/c$ by shifting the Au^{I} cations in successive bc layers such that they fall into the same ac plane and accommodate the aurophilic interactions (Figure 5, right). The resulting network appears to be poorly packed

Table 5. Relative energies (E_r = E_0 – E_i) and lattice parameters computed for three dynamically stable AuO polymorphs. The relative energies and volumes were calculated per formula unit. See text for details.

Structure	E_r [meV]	V [Å^3]	a [Å]	b [Å]	c [Å]	[°]	β [°]	[°]
Layered $P2_1/c$	105	29.7	3.341	6.871	5.388	90	74.2	90
AgO $P2_1/c$	42	29.3	5.857	3.782	5.644	90	110.5	90
			12.310[a]	3.783[a]	5.644[a]	90[a]	109.5[a]	72[a]
$C2/c$	0	32.1	12.843	3.919	5.535	90	112.8	90

[a] Transformed by matrix (2,1,0; 0,1,0; 0,0,1) for direct comparison with the $C2/c$ structure.

(as the view along *c* in Figure 5 top right reveals). The atomic rearrangements leading to the *C*2/*c* structure require opening of the γ angle by approximately 20° (in *C*2/*c* settings), whereas they have little impact on the remaining lattice vectors (Table 5). Significant departure from the ideal rock salt prototype, the presence of open channels, and the aurophilic interactions render the predicted *C*2/*c* form a unique structural type among the LTM monoxides—much like $AuSO_4$ is different from all other LTM sulfates. We find the enthalpy of formation of AuO to be –60 meV FU^{-1} (p = 1 atm) with respect to the elemental crystals α-O_2 and Au. In comparison, we calculated enthalpies of formation for Au_2O_3 and hypothetical Au_2O to be –345 and +551 meV FU^{-1}, respectively. These values are in qualitative agreement with previous DFT results.[38] The stability and structural changes in AuO as a function of external pressure will be discussed in future work.[39]

Conclusions

We have revisited the crystal structures of LTM monoxides and sulfates. Very few oxides in this class crystallize in a perfect ionic rock salt type cationic/anion lattice (typical rather of early transition metal oxides), but adopt many seemingly unrelated unit cells. However, their matrix-transformed unit cells reveal striking similarities to the prototypical rock salt type. Typically, the rock salt type representation yields tetragonally compressed (CuO, PdO, both forms of AgO) or elongated (HgO *Pnma* and $P\bar{1}$) cells, occasionally with small angular distortions of cell vectors. The heavy atom sublattice is usually less prone to distortions than the oxygen sublattice.

All but one of the 4d/5d LTM sulfates adopt tetragonally distorted rock salt lattices, thus resembling the corresponding oxides ($AuSO_4$ is the exception). The distortions of the MO and MSO_4 structures from the rock salt prototype may be understood as originating from collective JT distortions of the [MO_6] octahedra. The substantial covalent character of LTM–oxygen bonds,[11] which is most pronounced for the LTMs, the dominant role of JT distortions, and the (rotational) flexibility of sulfate anion are all jointly responsible for the remarkable crystallochemical similarity between the MO and MSO_4 systems.

By recognizing and exploiting the structural similarities between compounds of 4d and 5d metals, and also between oxides and sulfates, we were able to predict that $PtSO_4$ should exist in the $PdSO_4^{HT}$-type structure. More thorough structure searches for as of yet unknown AuO revealed the role of disproportionation and aurophilic interactions for the energetic stabilization of a unique *C*2/*c* polymorph. This predicted structural type of AuO is rather loosely packed, as it contains channels in the structure, and yet, it is energetically and dynamically stable.

Details of Computations

QM Calculations: The periodic DFT calculations were performed by using the Vienna ab initio simulation package (VASP)[40] within generalized gradient approximation (GGA)[41] PBEsol exchange–correlation functional revised for solids[42] and projector-augmented wave method (PAW).[43] Parameters for full geometry optimization were: SCF convergence criterion 10^{-7} eV, ionic convergence 10^{-5} eV, kpoint spacing of 0.4 Å^{-1} (0.25 Å^{-1} in case of the single-point energy calculations). By using the Monkhorst–Pack scheme, valence electrons were described by plane waves with a kinetic energy cutoff of 500 eV. The phonon dispersion calculations were performed by using the program PHONON[44] implanted into the materials design platform MedeA.[45] Structure searches for AuO by using evolutionary algorithms[46] were performed with the XtalOpt package[47] and Z = 4 formula units per unit cell. Total energies of structural candidates were evaluated by using the VASP package, the PBE exchange-correlation functional,[48] and a plane wave energy cutoff of 400 eV. The best structural candidates were reoptimized by using the parameters listed above.

Supporting Information (see footnote on the first page of this article): Joint classification of the MO/MS/MSO_4 compounds, fractional atomic displacements, and phonon dispersion curves.

Acknowledgments

W. G. acknowledges support from the project "AgCENT: New Unique Magnetic and Electronic Materials based on Compounds of Divalent Silver" from the Polish National Science Centre (NCN). DFT calculations were performed at ICM supercomputers within grant G29-3. A. H. and R. H. are grateful for support from EFree, an Energy Frontier Research Center funded by the U.S. Department of Energy (grant number DESC0001057 at Cornell) and from the U.S. National Science Foundation (NSF) (grant number CHE-0910623). Computational resources provided by the Cornell Nano-Scale Facility (supported by the U.S. National Science Foundation (NSF) through grant ECS-0335765), the XSEDE network (provided by the National Center for Supercomputer Applications through grant TG-DMR060055N), and the KAUST Supercomputing Laboratory (project ID k128) are gratefully acknowledged. M. D. and W. G. are grateful to Dr. Piotr Leszczyński for valuable discussions.

[1] The first-order JT effect refers to the situation of true orbital degeneracy, whereas the second-order (or pseudo-) JT effect operates for orbitals close to each other in energy [such as, for example, filled d(z^2) orbital and empty s orbital].
[2] See, for example, the long-standing problem of metallization of NiO, a classical Mott–Hubbard insulator: A. G. Gavriliuk, I. A. Trojan, V. V. Struzhkin, *Phys. Rev. Lett.* **2012**, *109*, 086402.
[3] These two phenomena may be discussed jointly by using the formalism of electron–phonon coupling.
[4] G. A. Slack, *J. Appl. Phys.* **1960**, *31*, 1571–1582.
[5] R. J. Poljak, *Acta Crystallogr.* **1958**, *11*, 306–306.
[6] L. Thomassen, *J. Am. Chem. Soc.* **1940**, *62*, 1134–1135.
[7] G. Tunell, E. Posnjak, C. J. Ksanda, *Z. Kristallogr.* **1935**, *90*, 120–142.
[8] M. Wildner, G. Giester, *Miner. Petrol.* **1988**, *39*, 201–209.
[9] K. Yoshio, A. Onodera, H. Satoh, N. Sakagami, H. Yamashita, *Ferroelectrics* **2001**, *264*, 133–138.
[10] C. H. Bates, W. B. White, *Science* **1962**, *137*, 993–993.
[11] M. Spiess, R. Gruehn, *Naturwissenschaften* **1978**, *65*, 594–594.
[12] W. J. Moore, L. Pauling, *J. Am. Chem. Soc.* **1941**, *63*, 1392–1394.
[13] T. Dahmen, P. Rittner, S. Böger-Seidl, R. Gruehn, *J. Alloys Compd.* **1994**, *216*, 11–19.
[14] A. G. Christy, S. M. Clark, *Phys. Rev. B* **1995**, *52*, 9259–9265.
[15] J. A. McMillan, *J. Inorg. Nucl. Chem.* **1960**, *13*, 28–31.

[16] M. Derzsi, A. Budzianowski, V. V. Struzhkin, P. J. Malinowski, P. J. Leszczyński, Z. Mazej, W. Grochala, *CrystEngComm* **2013**, *15*, 192–198.
[17] K. Yvon, A. Bezinge, P. Tissot, P. Fischer, *J. Solid State Chem.* **1986**, *65*, 225–230.
[18] H. P. Walmsley, *Proc. Phys. Soc. London* **1928**, *40*, 7–13.
[19] K. Aurivillius, C. Stalhandske, *Z. Kristallogr.* **1980**, *153*, 121–129.
[20] H. Liu, H. Mao, M. Somayazulu, Y. Ding, Y. Meng, D. Häusermann, *Phys. Rev. B* **2004**, *70*, 094114.
[21] J. Coing-Boyat, *Compt. Rendus* **1961**, *253*, 997–999.
[22] M. Spiess, R. Gruehn, *Z. Anorg. Allg. Chem.* **1979**, *455*, 16–28.
[23] K. Aurivillius, *Acta Chim. Scand.* **1964**, *18*, 1305–1306.
[24] P. A. Kokkoros, P. J. Rentzeperis, *Z. Kristallogr.* **1963**, *119*, 234–244.
[25] D. J. Benjamin, *Mater. Res. Bull.* **1982**, *17*, 179–189.
[26] K. Aurivillius, I. B. Carlsson, *Acta Chim. Scand.* **1957**, *11*, 1069–1069; K. Aurivillius, I. B. Carlsson, *Acta Chim. Scand.* **1958**, *12*, 1297–1304.
[27] T. Zhou, U. Schwarz, M. Hanfland, Z. X. Liu, K. Syassen, M. Cardona, *Phys. Rev. B* **1998**, *57*, 153–160.
[28] J. Yan, B. Chen, S. V. Raju, B. K. Godwal, A. A. MacDowell, J. Knight, H. Ma, Q. Williams, *Phys. Chem. Miner.* **2012**, *39*, 269–275.
[29] M. S. Wickleder, *Z. Anorg. Allg. Chem.* **2001**, *627*, 2112–2114.
[30] We adopt a convention that labels an "inverse" JT effect as a tetragonal compression of an octahedron, whereas the normal JT effect results in its elongation.
[31] P. Schwerdtfeger, J. Li, P. Pyykko, *Theor. Chim. Acta* **1994**, *87*, 313–320.
[32] See the discussion of the Pauling rules in oxides: F. C. Hawthorne, *Acta Crystallogr., Sect. B* **1994**, *50*, 481–510.
[33] J. P. Bastide, *J. Solid State Chem.* **1987**, *71*, 115–120. See also updated version: D. Errandonea, F. J. Manjón, *Prog. Mater. Sci.* **2008**, *53*, 711–773.
[34] D. J. Pettifor, *J. Phys. F: Metal Phys.* **1997**, *7*, 613; C. M. Varma, A. J. Wilson, *Phys. Rev. B* **1980**, *22*, 3795–3804; O. K. Andersen, O. Jepsen, D. Glötzel, *Highlights of Condensed Matter Theory* (Eds.: F. Bassani, F. Fumi, M. P. Tosi), North-Holland Publishing Company, Amsterdam, **1985**, p. 59–176.
[35] A. Vegas, M. Jansen, *Acta Crystallogr., Sect. B* **2002**, *58*, 38–51.
[36] D. C. Lonie, E. Zurek, *J. Comp. Physiol.* **2011**, *182*, 372–387.
[37] P. Pyykkö, Y. F. Zhao, *Angew. Chem.* **1991**, *103*, 622–623; *Angew. Chem. Int. Ed. Engl.* **1991**, *30*, 604–605.
[38] H. Shi, R. Asahi, C. Stampfl, *Phys. Rev. B* **2007**, *75*, 205125.
[39] A. Hermann, M. Derzsi, W. Grochala, R. Hoffmann, *manuscript in preparation*.
[40] G. Kresse, J. Furthmüller, *Comput. Mater. Sci.* **1996**, *6*, 15–50; G. Kresse, J. Furthmüller, *Phys. Rev. B* **1996**, *54*, 11169–11186.
[41] J. P. Perdew, K. Burke, M. Ernzerhof, *Phys. Rev. Lett.* **1996**, *77*, 3865–3868.
[42] J. P. Perdew, A. Ruzsinszky, G. I. Csonka, O. A. Vydrov, G. E. Scuseria, L. A. Constantin, X. Zhou, K. Burke, *Phys. Rev. Lett.* **2008**, *100*, 136406.
[43] P. E. Blöchl, *Phys. Rev. B* **1994**, *50*, 17953–17979; G. Kresse, J. Joubert, *Phys. Rev. B* **1999**, *59*, 1758–1775.
[44] K. Parliński, *Software PHONON*, Cracow, Poland, **2008**.
[45] http://www.materialsdesign.com/medea.
[46] B. J. Hartke, *Phys. Chem.* **1993**, *97*, 9973–9976; R. L. Johnston, *Dalton Trans.* **2003**, 4193–4207; A. R. Oganov, A. O. Lyakhov, M. Valle, *Acc. Chem. Res.* **2011**, *44*, 227–237.
[47] D. C. Lonie, E. Zurek, *J. Comp. Physiol.* **2011**, *182*, 2305–2306.
[48] J. P. Perdew, K. Burke, M. Ernzerhof, *Phys. Rev. Lett.* **1996**, *77*, 3865–3868.

Received: June 19, 2013
Published Online: August 21, 2013

